Materials Research Bulletin 133 (2021) 111022

Contents lists available at ScienceDirect

Materials Research Bulletin

journal homepage: www.elsevier.com/locate/matresbu

Vibrational spectroscopy and microwave dielectric properties of two novel $Ca_3Ln_2W_2O_{12}$ (Ln = La, Sm) tungstate ceramics

Bing Liu*, Kai Xin Song*

College of Electronic Information and Engineering, Hangzhou Dianzi University, Hangzhou 310018, China

ARTICLE INFO

Keywords:
$Ca_3Ln_2W_2O_{12}$
microwave dielectric properties
vibrational spectroscopy

ABSTRACT

Two novel tungstate ceramics with **a** nominal composition of $Ca_3Ln_2W_2O_{12}$ (Ln = La, Sm) were prepared via standard solid-state reaction methods. **According to** X-ray diffraction patterns, both ceramics crystallized in hexagonal crystal systems with **a** space group of $R\bar{3}m$ (No. 166). The vibrational modes of **the** Raman spectra were **identified**, and the evolutions of **the** wavenumber and **the** full width at half **maximum** (FWHM) were analyzed. The optimum microwave dielectric properties with ε_r = 18.7, Qf = 50,500 GHz, **and** τ_f =–90 ppm/°C were **realized** in $Ca_3La_2W_2O_{12}$ ceramics, while moderate Qf values were obtained in **the** Sm composition (ε_r = 19.5, Qf = 15,700 GHz**, and** τ_f =–95 ppm/°C). The discrepancy in **the** Qf values was associated with the broader FWHM of Raman spectra and smaller grain sizes. Infrared reflectivity (IR) spectra were also **used** to **determine** the intrinsic dielectric loss, where more damped phonon parameters were also **identified** in $Ca_3Sm_2W_2O_{12}$ ceramics.

1. Introduction

Over **the past** decades, in pace with the booming industry of microwave telecommunications, microwave dielectric ceramics have become indispensable components **of** various microwave devices due to their compactness, light weight, thermal stability, low cost and excellent performance [1]. From the device design **perspective**, dielectrics with **suitable values of the** dielectric constant (ε_r) are required **for balancing** device miniaturization and short signal delay time. A high Qf value (Q = 1/tanδ and f denotes the resonant frequency) can reduce the energy loss during signal propagation and create **satisfactory** frequency selectivity, which is of vital importance **to** minimizing the signal attenuation. **In addition**, a low temperature coefficient of resonant frequency (τ_f) is required **for ensuring** frequency stability. Last, for massive **industrial** production, the cost **effectiveness** is another important factor as the typical ultra-low-loss candidates, such as Ba-based complex perovskites, **typically** contain noble raw materials, such as tantalates or niobates [2,3]. **The identification of a single material that satisfies** all these requirements **is a formidable task**, and **optimally balancing these properties is a major challenge** in the microwave dielectric ceramics industry.

Tungstates have been **regarded** as important candidates for dielectric materials **due** to their low cost, facile synthesis, **satisfactory** chemical stability, and excellent dielectric properties. Among **tungstates**, AWO_4 (A = Ca, Sr, Ba, Zn, Co, **or** Ni) compounds with monoclinic wolframite or tetragonal scheelite structures are well known [4–7]. Pullar et al. reported that AWO_4 ceramics **that are** sintered at 1200 °C **typically** exhibit low dielectric constant **values** of **approximately** 12 and Qf values in the range of 24,900–62,800 GHz [4]. In 2011, Li_2WO_4 ceramics with **an** ultra-low sintering temperature of **approximately** 650 °C were reported by Zhou et al., and their **satisfactory** microwave dielectric properties (ε_r ~ 5.5, Qf ~ 62,000 GHz, **and** τ_f =–146 ppm/°C) indicated **high** potential in ultra-low-temperature cofired ceramic (ULTCC) technologies [8]. More recently, various **types** of tungstates such as Li_4WO_5, $LiAlW_2O_8$, and $Li_2Mg_2(WO_4)_3$ were proposed, and their potential applications in microwave dielectric ceramics were systematically investigated [9–11]. $Ca_3Ln_2W_2O_{12}$ (Ln = La **and** Sm) powders are widely applied as promising host materials for inorganic phosphors due to their outstanding structural tunability and luminescent properties [12–14]. However, to the best of our knowledge, **minimal investigation** has been conducted on the potential applications of $Ca_3Ln_2W_2O_{12}$ ceramics **or on** their microwave dielectric properties. Therefore, **the exploration of** the structural parameters and microwave dielectric properties of $Ca_3Ln_2W_2O_{12}$ ceramics **could be important**, and may trigger a new breakthrough in the **development of** novel tungstate-based microwave dielectric ceramics **that realize** high performances.

In this **study**, the crystal **structures and** Raman spectra of $Ca_3Ln_2W_2O_{12}$ ceramics are systematically investigated, together with their effects on the microwave dielectric properties. Moreover, IR

* Corresponding author.
E-mail addresses: liubing@hdu.edu.cn (B. Liu), kxsong@hdu.edu.cn (K.X. Song).

https://doi.org/10.1016/j.materresbull.2020.111022
Received 19 February 2020; Received in revised form 1 July 2020; Accepted 28 July 2020
Available online 31 July 2020
0025-5408/

spectra are extrapolated to **the** microwave frequency region to further **identify** the intrinsic dielectric properties.

2. Experimental procedure

$Ca_3Ln_2W_2O_{12}$ ceramics were prepared via high temperature solid-state reactions of $CaCO_3$ (99.99%), La_2O_3 (99.99%), Sm_2O_3 (99.99%) and WO_3 (99.99%) raw **powders**. **Prior to** weighing, La_2O_3 and Sm_2O_3 **were** preheated at 900 °C for 2 h to remove the moisture. The stoichiometric powder was ball-milled with zirconia media **at a speed of 180 r/min** for 6 h. After that, the obtained mixtures were calcined at 1100 °C for 3 h and pressed into cylindrical pellets **of** 12 mm in diameter and 5 mm in height. Finally, the pellets were sintered at 1300 °C-1400 °C for 3 h **at a heating rate of 5°C/min** to obtain the dense ceramics.

X-ray diffraction patterns **were** collected using **a** RIGAKU D/max 2550/PC. Scanning electron micrographs were obtained from the polished and **thermally** etched surfaces using **a** SIRION-100 **system**. Raman spectra were recorded **using an** HR-800 LabRaman device. IR spectra were collected using an IFS 66v/s infrared spectrometer. The relative densities were measured **via** the Archimedes method. The microwave dielectric properties were evaluated using **a silver-coated resonant cavity connected to** a vector network analyzer (E8363B, Agilent Technologies Inc., Palo Alto, CA) [15,16]. **The measurement of τ_f value was conducted in the temperature range of 20-80°C.**

3. Results and discussion

The XRD patterns of $Ca_3Ln_2W_2O_{12}$ ceramics **that were** sintered at 1300 °C are presented in Fig. 1(a). Both patterns exhibit similar diffraction features, and all the diffraction peaks can be well indexed according to the standard PDF card of $Ca_3La_2W_2O_{12}$ (JCPDS #49-0965). **Hence,** monophasic $Ca_3Ln_2W_2O_{12}$ ceramics have been successfully obtained in this **study.** Based on the cell refinements, the cell parameters of $Ca_3Ln_2W_2O_{12}$ ceramics are calculated as follows: $a = b = 9.76375$ Å, $c = 55.54702$ Å, $\gamma = 120°$ for La and $a = b = 9.75646$ Å, $c = 55.47817$ Å, **and** $\gamma = 120°$ for Sm. Moreover, **according to** the enlarged figure **in the** inset, the corresponding diffraction peaks of **the** Sm composition indicate higher 2θ than that of **the** La composition, which corresponds to cell shrinkage of **the** $Ca_3Sm_2W_2O_{12}$ ceramics. **Although** the crystal structure of $Ca_3Ln_2W_2O_{12}$ has not been reported yet, it is widely believed that it crystallizes in **a** hexagonal crystal system with a space group of $R\bar{3}m$, which is similar to that of $Ca_5Re_2O_{12}$ [17,18]. As approximately depicted in Fig. 1(b), the A-site cations (Ca^{2+} and Ln^{3+}) have four **types** of sites [coordination number (CN) = 6, 8, **and** 9], **while three types** of W^{6+} sites are observed and they are all located in the **centre** of **the** oxygen octahedra (CN = 6).

SEM images of the polished and **thermally** etched surfaces of $Ca_3Ln_2W_2O_{12}$ ceramics **that were** sintered at 1375 °C are shown in Fig. 2. Both samples exhibit dense **microstructures** with normal grain size distributions, and the grain exhibit **a** hexangular shape-like morphology. **The** average grain size of $Ca_3La_2W_2O_{12}$ (9.85 μm) is slightly larger than that of **the** Sm composition (8.26 μm). Moreover, no abnormal grain growth with **a** strong preferred orientation is observed, even though the crystal structure of **the** $Ca_3Ln_2W_2O_{12}$ ceramics **corresponds to** a large c/a value.

Room-temperature Raman spectra of **the** $Ca_3Ln_2W_2O_{12}$ ceramics are shown in Fig. 3(a). Strong similarities **are observed** when comparing the Raman spectra of the present ceramics with those of $Ca_3La_2Te_2O_{12}$, LiH_5TeO_6, **and** Bi_2WO_6, etc [18–20]. **The** Raman spectra of **the** $Ca_3Ln_2W_2O_{12}$ ceramics **exhibit** eight bands: a very strong high-frequency shoulder band at 780-860 cm^{-1}, two very weak and broad bands at 700-780 cm^{-1} and 480-540 cm^{-1}, two medium-intensity bands at **approximately** 445 and 287 cm^{-1} and three weak bands at **approximately** 368, 225, and 129 cm^{-1}. According to Poirier et al., the Raman bands at 500-900 cm^{-1} are assigned to the asymmetric and symmetric stretching vibrations of the bridging W-O-W bonds [20,21]. The two bands at **approximately** 445 and 368 cm^{-1} are typical characteristics **of** the bending vibrations of W-O terminal bonds in WO6 octahedra [22]. The **remaining** three low-frequency bands may be associated with the **nonsymmetric** bending of **the** Ca/La-O bond [23]. **With** substitution of smaller Sm^{3+} ($r = 0.958$ Å, CN = 6; $r = 1.079$ Å, CN = 8; $r = 1.132$ Å, and CN = 9) for La^{3+} ($r = 1.032$ Å, CN = 6; $r = 1.16$ Å, CN = 8; $r = 1.216$ Å, and CN = 9) [24], the Raman **spectrum** of $Ca_3Sm_2W_2O_{12}$ undergoes an overall **blueshift** compared with that of the La composition. By simplifying the lattice vibration as a harmonic resonant model, the corresponding wavenumbers (ω) could be correlated with the bond strength (k) and the reduced mass (m^*) using the following equation [25]:

$$\omega = \sqrt{k/m^*} \quad (1)$$

Fig. 3(b) **presents** the wavenumber differences ($\triangle\omega = \omega_{Sm} - \omega_{La}$) of the labeled Raman peaks **(peaks** A-G). As the atomic mass of Sm is larger than **that of** La, the positive $\triangle\omega$ values in Fig. 3(b) indicate that the bond strength (k) of $Ca_3Sm_2W_2O_{12}$ ceramics should be stronger than that of **the** La composition. Therefore, it is reasonable to infer that the vibration bonds of $Ca_3Ln_2W_2O_{12}$ could be more compressed after the rational substitution of Sm for La. Moreover, FWHM of **the** Raman peak has been widely accepted as an important indicator of microwave dielectric properties, and the broadening of FWHM could be closely related to the decay of microwave propagation [26–28]. The FWHM differences of the present ceramics ($\triangle FWHM = FWHM_{(Sm)} - FWHM_{(La)}$) are **presented** in Fig. 3(c). **Except for** the split peak at ~820 cm^{-1} (peak G), all the Raman peaks of **the** $Ca_3Sm_2W_2O_{12}$ ceramics are

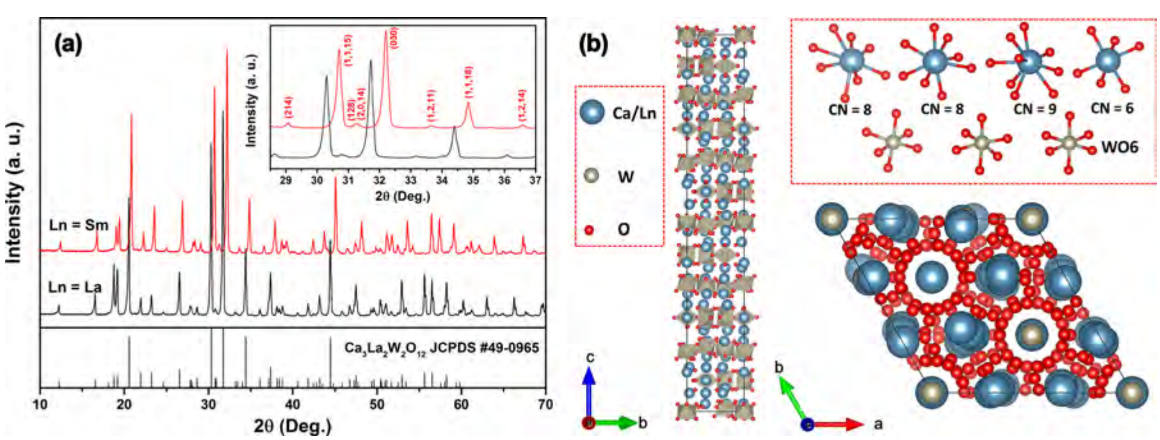

Fig. 1. (a) XRD patterns of $CaLn_2W_2O_{12}$ ceramics (Ln = La, Sm). (b) Schematic **illustrations** of the approximate crystal structure of $Ca_3Ln_2W_2O_{12}$ ceramics and the coordination environments of the cations.

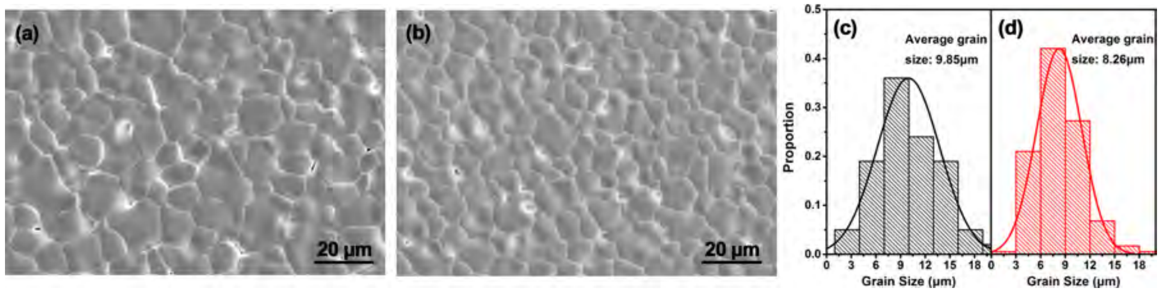

Fig. 2. SEM images and grain size distributions of (a,c) $Ca_3La_2W_2O_{12}$ and (b,d) $Ca_3Sm_2W_2O_{12}$ ceramics **that were** sintered at 1375 °C.

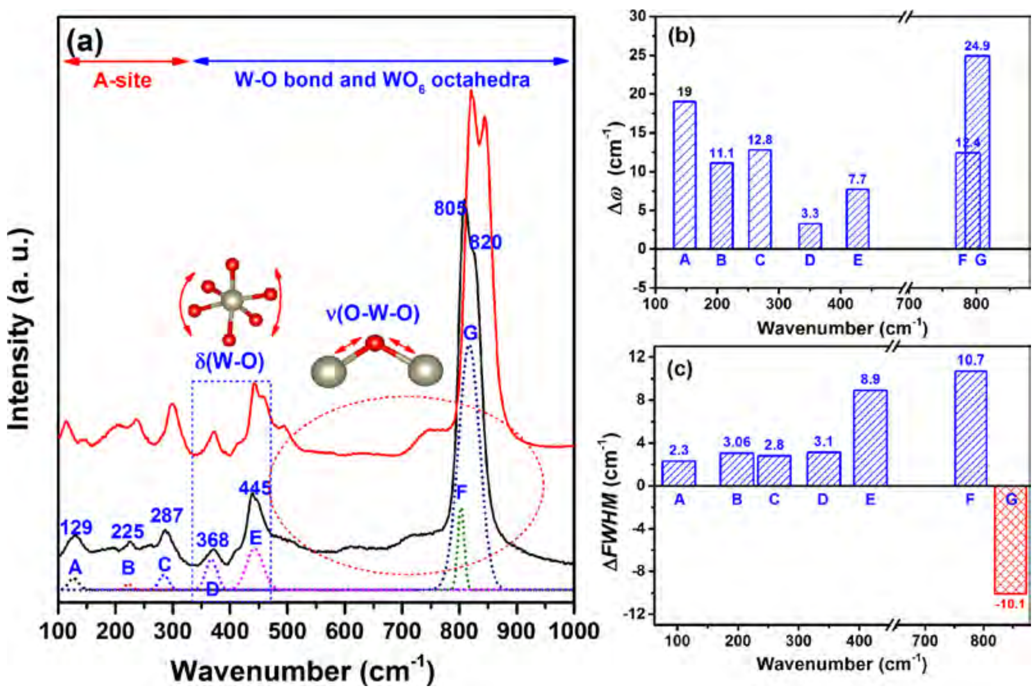

Fig. 3. (a) Raman spectra of $Ca_3Ln_2W_2O_{12}$ ceramics and the differences **in the** (b) wavenumber and (c) FWHM **between** La and Sm compositions. *Note.* Abbreviations: ν, stretching; δ, deformation, or bending.

widened compared with the corresponding peaks in **the** La composition.

The variations of **the** relative density and **the** microwave dielectric properties are **presented** in Fig. 4. The relative densities of both ceramics increase monotonously with increasing sintering temperature until they reach the maximum values of above 0.95 at 1375 °C and degrade slightly thereafter. The **variation** trends of **the** ε_r values are in **satisfactory** agreement with those of the relative densities. **Hence,** the porosity should be the dominant factor in controlling ε_r. To **exclude** the impact of porosity (*P*), the following empirical equation, **which was** proposed by Alford et al., is **used** to **determine** the actual dielectric constant (ε_m) [29]:

$$\varepsilon_r = \varepsilon_m(1 - \frac{3P(\varepsilon_m - 1)}{2\varepsilon_m + 1}) \tag{2}$$

The variation of the calculated ε_m values is plotted in Fig. 4(b). **The** ε_m values are located **mainly** at **approximately** 20 and vary indistinctively with increasing sintering temperature. **This** further **demonstrates** the important role of **the** relative density in determining the resultant dielectric constant. **The** *Qf* values of $Ca_3Ln_2W_2O_{12}$ ceramics increase monotonously with **the** increasing sintering temperature until the maximum values of 50,500 GHz for $Ca_3La_2W_2O_{12}$ and 15,700 GHz for $Ca_3Sm_2W_2O_{12}$ **are attained** at 1375 °C. **The** τ_f values of the present ceramics v**ary around -90 ppm/°C and** indicate slight downward **variation** trends with increasing sintering temperature (see Fig. 4(d)). **To further adjust the temperature stability, adding compounds with high positive τ_f value, such as TiO_2 (+450 ppm/°C)** [30], **should be effective and is now in progress**. The **optimal** combinations of **the** microwave dielectric properties are **identified** as follows: ε_r = 18.7, *Qf* = 50,500 GHz, **and**τ_f =–90 ppm/°C for $Ca_3La_2W_2O_{12}$ and ε_r = 19.5, *Qf* = 15,700 GHz, **and** τ_f =–95 ppm/°C for $Ca_3Sm_2W_2O_{12}$.

Notoriously, the variation of **the** *Qf* values can be explained **by** both intrinsic factors (such as structural symmetry **and** ionic/electronic polarizability) and extrinsic factors (**microstructural** flaws, such as porosity, grain boundary and secondary phase) [31,32]. For the extrinsic part, the effects of **a** secondary phase can be excluded as monophasic compositions have been **demonstrated by** the XRD results. Hence, the extrinsic dielectric loss should be mainly discussed in terms of **the** porosity, grain boundary, **and electrical conductivity** [33]. For each composition, **the** *Qf* value indicates an overall improvement with increasing sintering temperature, which corresponds to the decline of **the** porosity. **The** larger average grain size of $Ca_3La_2W_2O_{12}$ ceramics should be a key extrinsic factor for their much higher *Qf* value. **The variation of electrical conductivity and its effect on the resultant *Qf* values could be evaluated via measuring the impedance under various temperature, which needs to be further investigated.** Furthermore, for the intrinsic part, the overall larger FWHM of $Ca_3Sm_2W_2O_{12}$ ceramics should **correspond to** a more damped lattice vibration, which could play an important role in their intrinsic dielectric loss.

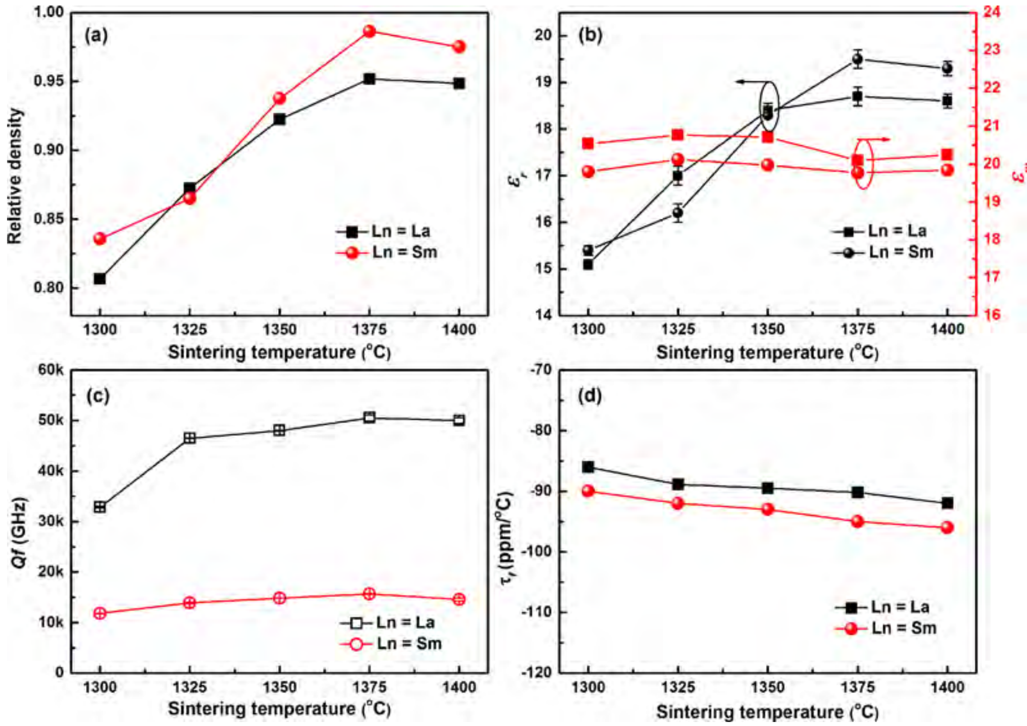

Fig. 4. (a) **The** relative density and (b-d) **the** microwave dielectric properties of $Ca_3Ln_2W_2O_{12}$ ceramics as functions of **the** sintering temperature.

Table 1
Phonon parameters that were calculated by fitting the IR spectra of $Ca_3Ln_2W_2O_{12}$ (Ln = La, Sm) ceramics.

La	ω_j(cm^{-1})	γ_j(cm^{-1})	$\triangle\varepsilon_j$	$\triangle\tan\delta_j \times 10^4$ at 10GHz	Sm	ω_j(cm^{-1})	γ_j(cm^{-1})	$\triangle\varepsilon_j$	$\triangle\tan\delta_j \times 10^4$ at 10GHz
1	177.0	42.6	5.2	1.1777	1	175.8	54.8	6.9	2.1982
2	210.0	58.1	2.2	0.3253	2	238.3	63.5	1.8	0.3246
3	303.0	39.7	2.5	0.1923	3	306.6	35.9	2.9	0.2078
4	330.3	31.0	2.4	0.1205	4	335.1	30.5	1.7	0.0812
5	363.4	33.5	0.7	0.0314	5	365.5	26.6	0.5	0.0119
6	468.9	46.6	0.3	0.0101	6	464.9	39.9	0.2	0.0077
7	573.4	38.7	0.6	0.0130	7	575.0	49.4	0.7	0.0193
8	628.5	120.6	0.5	0.0313	8	645.6	81.9	0.4	0.0090
9	820.2	101.8	0.01	0.0001	9	848.6	80.4	0.1	0.0013
ε_∞			4.2	0.0000	ε_∞			4.2	0.0000
Σ			18.61	1.9017	Σ			19.4	2.9303

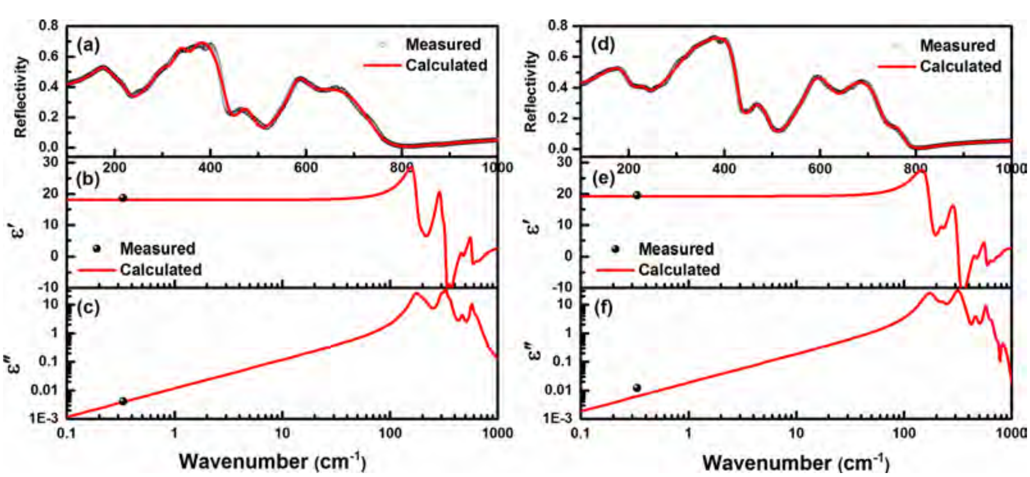

Fig. 5. Measured and calculated IR spectra of (a) $Ca_3La_2W_2O_{12}$ and (d) $Ca_3Sm_2W_2O_{12}$ ceramics and the real (ε') and imaginary parts (ε'') of the complex dielectric constants of (b,c) $Ca_3La_2W_2O_{12}$ and (e,f) $Ca_3Sm_2W_2O_{12}$ ceramics sintered at 1375 °C.

To further **investigate** the intrinsic dielectric properties, IR spectra of $Ca_3Ln_2W_2O_{12}$ ceramics **sintered at 1375°C is** fitted according to the phonon parameters **that are** listed in Table 1. The fitting method has been described in detail in our previous **studies** [25,31]. **In the** infrared frequency region, extrinsic factors will **not affect** the dielectric responses, and the calculated values from IR spectra can **be used to** distinguish the intrinsic dielectric properties from the measured **dielectric properties**. As shown in Fig. 5(a, d), the fitted spectra **well accord with** the measured spectra. Moreover, the calculated real (ε') and imaginary (ε'') parts of the complex dielectric constant are plotted and compared with the calculated **values** (black circles) (see Fig. 5(b,e) and (c,f)). The calculated and measured dielectric losses are **of** the same order of magnitudes (see Fig. 5(c,f)). **Hence,** the intrinsic dielectric loss should play a leading role in the overall dielectric losses. Moreover, the calculated intrinsic dielectric loss ($\Sigma\tan\delta_j$) of $Ca_3Sm_2W_2O_{12}$ (2.9303×10^{-4}) is much higher than that of **the** La composition (1.9017×10^{-4}), which corresponds to the lower measured *Qf* values in $Ca_3Sm_2W_2O_{12}$ ceramics. According to Table 1, this is mainly due to the more damped phonon mode at ~175 cm^{-1}, and the contributions from higher frequency modes decrease rapidly with increasing ω_j **since** $\triangle\varepsilon_j \sim S_j\omega_j^{-2}$ and $\triangle\tan\delta_j \sim \omega S_j\gamma_j\omega_j^{-4}$ [34].

4. Conclusions

Two novel tungstate ceramics with **a** nominal composition of $Ca_3Ln_2W_2O_{12}$ (Ln = La, Sm) have been prepared via standard solid-state reaction methods. **The** XRD results **demonstrate** the formation of monophasic $Ca_3Ln_2W_2O_{12}$ ceramics with **a** space group of $R\bar{3}m$. Dense microstructures with **a** hexangular-shape-like grain morphology are obtained when sintered at 1375 °C, where the optimal microwave dielectric properties (ε_r = 18.7, *Qf* = 50,500 GHz**, and** τ_f =–90 ppm/°C) are also **realized** in $Ca_3La_2W_2O_{12}$ ceramics. **The** ε_r and τ_f values of $Ca_3Sm_2W_2O_{12}$ ceramics are similar **to those** of **the** La composition, while their **optimal** *Qf* value (15,700 GHz) is much lower. The discrepancy in **the** *Qf* values is **also demonstrated by** the broader Raman peaks and more damped phonon parameters **that are obtained by fitting the** IR spectra.

Declaration of Competing Interest

The authors declare that they have no known competing financial interests or personal relationships that could have appeared to influence the work reported in this paper.

Acknowledgements

Financial support from the National Natural Science Foundation of China under grants numberS 51802062 and 51672063 is greatly appreciated.

References

[1] M.T. Sebastian, R. Ubic, H. Jantunen, Low-loss dielectric ceramic materials and their properties, Int. Mater. Rev. 60 (2015) 392–412.
[2] T. Shimada, Far-infrared reflection and microwave properties of $Ba[(Mg_{1-x}Zn_x)_{1/3}Ta_{2/3}]O_3$ ceramics, J. Eur. Ceram. Soc. 24 (2004) 1799–1803.
[3] S. Kawashima, M. Nishida, I. Ueda, H. Ouchi, $Ba(Zn_{1/3}Ta_{2/3})O_3$ ceramics with low dielectric loss at microwave frequencies, J. Am. Ceram. Soc. 66 (2010) 421–423.
[4] R.C. Pullar, S. Farrah, N. McN, Alford, $MgWO_4$, $ZnWO_4$, $NiWO_4$ and $CoWO_4$ microwave dielectric ceramics, J. Eur. Ceram. Soc. 27 (2007) 1059–1063.
[5] L. Cheng, Peng Liu, S.X. Qu, H.W. Zhang, Microwave dielectric properties of AWO_4 (A = Ca, Ba, Sr) ceramics synthesized via high energy ball milling method, J. Alloy Compd. 581 (2013) 553–557.
[6] N. Khobragade, E. Sinha, S.K. Rout, M. Kar, Structural, optical and microwave dielectric properties of $Sr_{1-x}Ca_xWO_4$ ceramics prepared by the solid state reaction route, Ceram. Int. 39 (2013) 9627–9635.
[7] J. Guo, D. Zhou, H. Wang, X. Yao, Microwave dielectric properties of (1−x) $ZnMoO_4$–$xTiO_2$ composite ceramics, J. Alloy Compd. 509 (2011) 5863–5865.
[8] D. Zhou, C.A. Randall, L.X. Pang, H. Wang, J. Guo, G.Q. Zhang, X.G. Wu, L. Shui, X. Yao, Microwave dielectric properties of Li_2WO_4 ceramic with ultra-low sintering temperature, J. Am. Ceram. Soc. 94 (2011) 348–350.
[9] J. Li, L. Fang, H. Luo, J. Khaliq, Y. Tang, C. Li, $_4LiWO_5$: A temperature stable low-firing microwave dielectric ceramic with rock salt structure, J. Eur. Ceram. Soc. 36 (2016) 243–246.
[10] X. Bai, P. Liu, Z. Fu, Q. Feng, L. Zhao, $LiAlW_2O_8$: A novel temperature stable low-firing microwave dielectric ceramic, Mater. Lett. 178 (2016) 68–70.
[11] J. Zhang, R. Zuo, Synthesis and microwave dielectric properties of $Li_2Mg_2(WO_4)_3$ ceramics, Mater. Lett. 158 (2015) 92–94.
[12] H.D. Autenrieth, S. Kemmler-Sack, Sensibilisierte IR-Emission der Dreiwertigen Seltenen Erden in $Ca_3La_2W_2O_{12}$, J. Solid State Chem. 58 (1985) 335–341.
[13] H.D. Autenrieth, S. Kemmler-Sack, W. Wischert, Lumineszenz und sensibilisierte Emission der dreiwertigen Seltenen Erden in $Ca_3La_2W_2O_{12}$, phys. status solidi (a) 83 (1984) 631–636.
[14] H.D. Autenrieth, S. Kemmler-Sack, Lumineszenz von $Ca_3La_2W_2O_{12}$: Mn und $Ca_3La_2Te_2O_{12}$: Mn, Mater. Chem. Phys. 12 (1985) 437–442.
[15] B.W. Hakki, P.D. Coleman, A dielectric resonant method of measuring inductive capacitance in the millimeter range, IRE Trans. Microwave Theory Tech. 8 (1960) 402–410.
[16] D. Kajfez, A. Gundavajhala, Measurement of material properties with a tunable resonant cavity, Electro. Lett. 29 (1993) 1936–1937.
[17] K. Li, R.V. Deun, Enhancing the energy transfer from Mn^{4+} to Yb^{3+} via a Nd^{3+} bridge role in $Ca_3La_2W_2O_{12}$: Mn^{4+},Nd^{3+},Yb^{3+} phosphors for spectral conversion of c-Si solar cells, Dyes and Pigments 162 (2019) 990–997.
[18] K. Li, R.V. Deun, $Ca_3La_2Te_2O_{12}$:Mn^{4+},Nd^{3+},Yb^{3+}: an efficient thermally-stable UV/visible–far red/NIR broadband spectral converter for c-Si solar cells and plant-growth LEDs, Mater. Chem. Front. 3 (2019) 403–413.
[19] L. Vanek, I. Nemec, I. CmHsarova, Z. Micka, V. Fajnor, A new lithium hydrogen tellurite–LiH_5TeO_6, J. Solid State Chem. 150 (2000) 410–415.
[20] M. Maczka, J. Hanuza, W. Paraguassu, A.G.S. Filho, P.T.C. Freire, J.M. Filho, Phonons in ferroelectric Bi_2WO_6: Raman and infrared spectra and lattice dynamics, Appl. Phys. Lett. 92 (2008) 112911.
[21] G. Poirier, Y. Messaddeq, S.J.L. Ribeiro, M. Poulain, Structural study of tungstate fluorophosphate glasses by Raman and X-ray absorption spectroscopy, J. Solid State Chem. 178 (2005) 1533–1538.
[22] Y. Li, J. Liu, X. Huang, J. Yu, Carbon-modified Bi_2WO_6 nanostructures with improved photocatalytic activity under visible light, Dalton Trans. 39 (2010) 3420–3425.
[23] I.Z. Hager, R. El-mallawany, M. Poulain, Infrared and Raman spectra of new molybdenum and tungsten oxyfluoride glasses, J. Mater. Sci. 34 (1999) 5163–5168.
[24] R.D. Shannon, Revised effective ionic radii and systematic studies of interatomic distances in halides and chalcogenides, Acta Crystallogr. A32 (1976) 751–767.
[25] B. Liu, L. Li, X.Q. Liu, X.M. Chen, Structural evolution of $SrLaAl_{1-x}(Zn_{0.5}Ti_{0.5})_xO_4$ ceramics and effects on their microwave dielectric Properties, J. Mater. Chem. C 4 (2016) 4684–4691.
[26] B. Liu, Y.H. Huang, K.X. Song, L. Li, X.M. Chen, Structural evolution and microwave dielectric properties in $Sr_2(Ti_{1-x}Sn_x)O_4$ ceramics, J. Eur. Ceram. Soc. 38 (2018) 3833–3839.
[27] F. Zhao, Z. Yue, Z. Gui, L. Li, Preparation, characterization and microwave dielectric properties of A_2BWO_6 (A = Sr, Ba; B = Co, Ni, Zn) double perovskite ceramics, Jpn. J. Appl. Phys. 44 (2005) 8066–8070.
[28] C.T. Chia, Y.C. Chen, H.F. Cheng, I.N. Lin, Correlation of microwave dielectric properties and normal vibration modes of $xBa(Mg_{1/3}Ta_{2/3})O_3$–$(1-x)Ba(Mg_{1/3}Nb_{2/3})O_3$ ceramics: I. Raman spectroscopy, J. Appl. Phys. 94 (2003) 3360–3364.
[29] S.J. Penn, N.M. Alford, A. Templeton, X.R. Wang, M.S. Xu, M. Reece, K. Schrapel, Effects of porosity and grain size on the microwave dielectric properties of sintered alumina, J. Am. Ceram. Soc. 80 (1997) 1885–1888.
[30] Y.H. Huang, B. Liu, K.X. Song, Microwave dielectric properties of temperature stable $(1-x)SrLaAlO_4$-$xTiO_2$ composite ceramics, Ceram. Int. 44 (2018) S125–S128.
[31] B. Liu, C.C. Hu, Y.H. Huang, H.B. Bafrooei, K.X. Song, Crystal structure, infrared reflectivity spectra and microwave dielectric properties of $CaAl_2O_4$ ceramics with low permittivity, J. Alloy Compd. 791 (2019) 1033–1037.
[32] Z. Wang, C. Yuan, B. Zhu, Q. Feng, F. Liu, J. Xu, C. Zhou, G. Chen, Sintering behavior, phase evolutions and microwave dielectric properties of $LaGaO_3$-$SrTiO_3$ ceramics modified by CeO_2 additives, Ceram. Int. 44 (2018) 6601–6606.
[33] M. Li, A. Feteira, M. Mirsaneh, S. Lee, M.T. Lanagan, C.A. Randall, D.C. Sinclair, Influence of nonstoichiometry on extrinsic electrical conduction and microwave dielectric loss of $BaCo_{1/3}Nb_{2/3}O_3$ ceramics, J. Am. Ceram. Soc. 93 (2010) 4087–4095.
[34] X.C. Fan, X.M. Chen, X.Q. Liu, Structural dependence of microwave dielectric properties of $SrRAlO_4$ (R = Sm, Nd, La) ceramics: crystal structure refinement and infrared reflectivity study, Chem. Mater. 20 (2008) 4092–4098.